1996-12

Non-electro-optic methods of high frequency laser modulation

Darwood, Joseph W.

Monterey, California. Naval Postgraduate School

NAVAL POSTGRADUATE SCHOOL
Monterey, California

THESIS

NON-ELECTRO-OPTIC METHODS OF HIGH FREQUENCY LASER MODULATION

by

Joseph W. Darwood

December, 1996

Thesis Advisors: Andrés Larraza
D. Scott Davis

Approved for public release; distribution is unlimited.

REPORT DOCUMENTATION PAGE

Form Approved OMB No. 0704-0188

1. AGENCY USE ONLY *(Leave blank)*	2. REPORT DATE December 1996.	3. REPORT TYPE AND DATES COVERED Master's Thesis

4. Non-Electro-optic Methods of High Frequency Laser Modulation

5. FUNDING NUMBERS

6. AUTHOR(S)
Darwood, Joseph W.

7. PERFORMING ORGANIZATION NAME(S) AND ADDRESS(ES)
Naval Postgraduate School
Monterey CA 93943-5000

8. PERFORMING ORGANIZATION REPORT NUMBER

9. SPONSORING/MONITORING AGENCY NAME(S) AND ADDRESS(ES)

10. SPONSORING/MONITORING AGENCY REPORT NUMBER

11. SUPPLEMENTARY NOTES The views expressed in this thesis are those of the author and do not reflect the official policy or position of the Department of Defense or the U.S. Government.

12a. DISTRIBUTION/AVAILABILITY STATEMENT
Approved for public release; distribution is unlimited.

12b. DISTRIBUTION CODE

13. ABSTRACT *(maximum 200 words)*

Two high frequency, non-electro-optic methods for modulating the intensity of a laser are examined theoretically and experimentally. The first modulation technique makes use of the Zeeman effect. Under an applied DC magnetic field, a splitting into two lines or three lines occurs. Modulation rates of 200 MHz have been proven possible with this technique. In the second technique, the properties of self-phase modulation of a monochromatic light are explored. For a high intensity beam, the optical path of a beam can be altered due the dependence of the phase on intensity. Thus two coherent beams of light of different intensity can be made to constructively or destructively interfere even if the physical paths are identical. In a configuration called a nonlinear-optical loop mirror, the output beam is amplitude modulated by linear variations in time of the total input power. A new design for a variable X-coupler, a key element of the loop mirror, is presented. Applications of high frequency modulators to test a theory of the AM–FM conversion of monochromatic light in fibers, to improve pulse rate control during target acquisition, and to high speed communications are discussed.

14. SUBJECT TERMS: High frequency Laser modulation, non-electro-optic Laser modulation	15. NUMBER OF PAGES 66
	16. PRICE CODE

17. SECURITY CLASSIFICATION OF REPORT	18. SECURITY CLASSIFICATION OF THIS PAGE	19. SECURITY CLASSIFICATION OF ABSTRACT	20. LIMITATION OF ABSTRACT
Unclassified	Unclassified	Unclassified	UL

NSN 7540-01-280-5500

Standard Form 298 (Rev. 2-89)
Prescribed by ANSI Std. 239-18 298-102

Approved for public release; distribution is unlimited.

NON-ELECTRO-OPTIC METHODS OF HIGH FREQUENCY LASER MODULATION

Joseph W. Darwood
Lieutenant Commander, United States Navy
B.S., University of Washington, 1983

Submitted in partial fulfillment
of the requirements for the degree of

MASTER OF SCIENCE IN APPLIED PHYSICS

from the

NAVAL POSTGRADUATE SCHOOL
December 1996

Author: [redacted]
Joseph W. Darwood

Approved by: [redacted]
Andrés Larraza, Thesis Advisor

[redacted]
D. Scott Davis, Thesis Advisor

[redacted]
Anthony A. Atchley, Chairman
Department of Physics

ABSTRACT

Two high frequency, non-electro-optic methods for modulating the intensity of a laser are examined theoretically and experimentally. The first modulation technique makes use of the Zeeman effect. Under an applied DC magnetic field, a splitting into two lines or three lines occurs. Modulation rates of 200 MHz have been proven possible with this technique. In the second technique, the properties of self-phase modulation of a monochromatic light are explored. For a high intensity beam, the optical path of a beam can be altered due the dependence of the phase on intensity. Thus two coherent beams of light of different intensity can be made to constructively or destructively interfere even if the physical paths are identical. In a configuration called a nonlinear-optical loop mirror, the output beam is amplitude modulated by linear variations in time of the total input power. A new design for a variable X-coupler, a key element of the loop mirror, is presented. Applications of high frequency modulators to test a theory of the AM–FM conversion of monochromatic light in fibers, to improve pulse rate control during target acquisition, and to high speed communications are discussed.

TABLE OF CONTENTS

I. INTRODUCTION

Due to self-interaction effects, the frequency of a wave in a dispersive medium is amplitude dependent, and in the weakly nonlinear regime it is of the form

$$\omega(k) = \omega_0(k) + \omega_2(k)e. \qquad (1\text{-}1)$$

In Eq. (1-1), $\omega_o(k)$ is the linear dispersion relation, $\omega_2(k)$ is the nonlinear coefficient, and e is the energy density which is proportional to the square of the wave amplitude. For the case of fixed frequency, positive group velocity, and $\omega_2 > 0$, the effect of nonlinearity is to decrease the wavenumber k as the amplitude of the wave field increases.

To understand the combined effects of dispersion and nonlinearity, we follow closely the physical argument given by Larraza and Coleman (Larraza, 1994). Consider an initial state of a modulated wave observed in a frame moving with the group velocity (Figure 1-1a). An observer in this frame would see the crests of the wave propagate. Because of dispersion, the group and phase velocities are different.

Consider now the case where the nonlinear coefficient $\omega_2 > 0$. An observer in the frame moving with the linear group velocity would observe bunching of the crests when the modulation amplitude is low and anti-bunching

when the modulation amplitude is high (Figure 1-1b). For positive dispersion, $\omega''(k)>0$,

$$\delta v_g = \omega''(k)\delta k \qquad (1\text{-}2)$$

increases towards the troughs of the modulation. Dispersive effects cause the energy to approach the troughs of the envelope, and the modulation propagates. Thus, to an observer moving with the linear group velocity, the modulation is no longer stationary. Instead, the modulation can propagate with a velocity that is either higher or lower than the linear group velocity. This result is general when the product $\omega_2\omega''$ is positive.

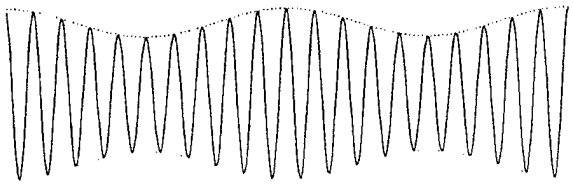

(a)

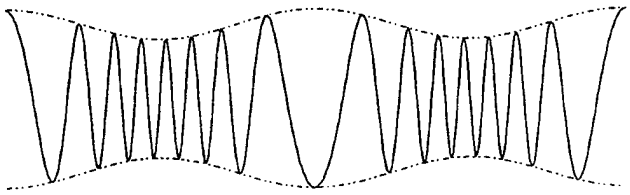

(b)

Figure 1-1. Modulated waves. a) Initial state of a modulated wave in the frame moving with the group velocity v_g. b) For positive dispersion, $\omega''(k)$ >0 and ω_2 > 0, δv_g increases toward the troughs of the modulation and the modulation propagates.

The stability of the modulation has the important consequence of providing a means for AM-FM conversion. This effect can be physically understood by considering again a modulated wave in a frame moving with the linear group velocity (Figure 1-2a). Assume that both the dispersion and the nonlinear coefficient ω_2 are negative. This is consistent with propagation of visible light in glass fibers. Due to nonlinear effects, an observer at a fixed location in this frame would see, after some time, alternating bunching and anti-bunching of the wave crests (Figure 1-2b). Because dispersive effects cause the energy to approach the troughs of the envelope, for this observer it would appear that at some time later the initial amplitude modulation has become a frequency modulation (Figure 1-2c). Dispersive effects would again remove energy from the region where the crests are more spread apart to the region where the crests are closer together. For the observer fixed in the frame moving with the group velocity it would appear that an amplitude modulation is superimposed upon the frequency modulated signal (Figure 1-2d). Nonlinearity will prevent an overshoot of energy flow to the crest of the modulation, and an amplitude modulation 180^{o} out of phase with respect to the original signal results at a later time (Figure 1-2e). In the frame moving with the group velocity, the process repeats periodically, and an observer in this frame sees that the modulations experience beats. In the laboratory frame, if a source is generating

an amplitude modulated signal, some distance away it will become frequency modulated.

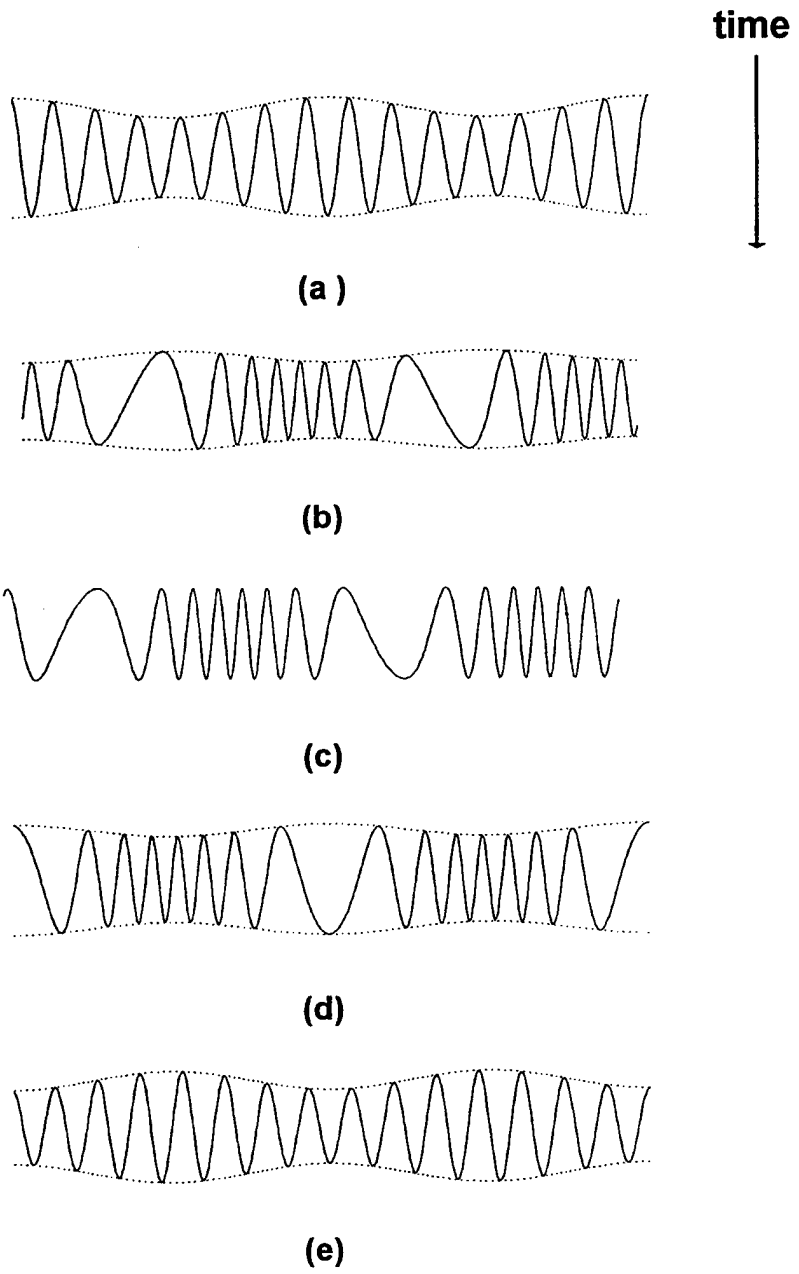

Figure 1-2. Time evolution of modulation. An observer in a frame moving with the linear group velocity observes AM–FM conversion in time.

Larraza and Coleman also give a quantitative theory for this effect. They have shown that an amplitude modulated signal with amplitude $\sqrt{e_0}$, modulation amplitude m, modulation frequency Ω, and carrier frequency ω will evolve according to

$$a(x,t) = \sqrt{e_0}\left[1 + m\cos(\Delta x)\cos(\Omega t - \eta x)\right]$$

$$* \cos\left[k_0 x - \omega t - \frac{2m\omega_o'}{\Omega}\sqrt{\frac{\omega_2 e_0}{\omega_o''}}\sin(\Delta x)\cos(\Omega t - \eta x)\right], \qquad (1\text{-}3)$$

where $\Delta = \Omega\sqrt{\omega_0'' \omega_2 e_0}/\omega_0'^2$.

A possible application of this result is broadband tunable lasers using fiber optics. Here, we are interested in single mode fibers consisting of a glass core of high index of refraction surrounded by a cladding with a lower index of refraction (about 0.1% smaller). In this case, for light in the visible range, the dispersion is normal, with $\omega_o''(k) < 0$. For light with intensity I, the index of refraction is given by $n(I) = n_0(\omega) + n_2 I$, where $n_o \approx 1.5$. Thus, the frequency nonlinear coefficient $\omega_2 \approx -\alpha n_2 \omega_o / n$ is negative, where α is a numerical factor of order unity. The order of magnitude of the coefficient n_2 (in units of cm^2/W) is about 10^{-11} or higher in rare earth doped glasses. (See Chapter II for details)

Because the product $\omega_o''(k)\omega_2 > 0$, the physical picture presented above applies to this case. In particular, for a 0.1 W source operating at a frequency of

5.8×10^{14} Hz and a 50% amplitude modulation of 10^{10} Hz in a 10 mm^2 fiber, the distance $x_m = p/2D$ for AM–FM conversion is about 20 m in doped glasses. The corresponding FM frequency spectrum has a range of about 3.5×10^{14} Hz in doped glasses. Thus, in doped glasses, amplitude modulated green light alternating between bright and dim at the source should alternate between red and blue at a rate of 10^{10} Hz at a location about 20 m down the fiber. This mechanism allows the possibility of producing tunable phased–locked coherent light from a single frequency coherent source.

Previous work has examined the characteristics of the argon-ion laser (Wallace, 1996) and an electro-optic method of modulating the laser using a commercially available modulator (Ladner, 1996). Modulation frequencies of 125 MHz with 25% modulation were achieved using the electro-optic method of modulation. The range of modulation frequencies achievable by this method appears to be limited to a range that is well below that desired. It also has inherent problems associated with the transmission and coupling of VHF power from the driving electronics to the modulator.

The purpose of this thesis is to investigate alternate means of amplitude modulation. This thesis research specifically examines two methods of amplitude modulation which do not require electro-optics. The first method uses the Zeeman effect to split a doublet lasing line into two separate but close frequencies inside the lasing cavity. The second method uses a non-linear

optical loop mirror, which induces a self phase modulation of a single input split into two non-equal components. The complete theory of these methods is given in Chapter II. In Chapter III we give details of the experimental setup and the experimental results. Chapter IV provides conclusions and recommendations for further experiments leading toward the desired modulation required for the AM-FM conversion theory to be tested.

II NON-ELECTRO-OPTIC MODULATION THEORIES

A. INTRODUCTION

In this chapter we investigate the theoretical limits of two modulation techniques that are not electro-optical in nature. The first modulation technique is magneto-optical and makes use of the DC Zeeman effect. Under an applied magnetic field, the orbital-spin degeneracy of most of the lasing medium's energy levels are broken and a splitting into two lines (longitudinal Zeeman effect) or three lines (transverse Zeeman effect) occurs. For the longitudinal Zeeman effect, if the transitions are within the gain curve of the laser, the result will be a beat pattern of the light intensity whose beating frequency is proportional to the applied magnetic field. In the case of the transverse Zeeman effect, the split spectrum is similar to that of amplitude modulation.

In the second technique, the properties of self-phase modulation of a monochromatic light are explored. For a high intensity beam, the nonlinearities of the medium cannot be neglected and the optical path of a beam can be altered due the dependence of the phase on intensity. Thus two coherent beams of light of different intensity can be made to constructively or destructively interfere even if the physical paths are identical. In a configuration called the nonlinear-optical loop mirror, the output beam is amplitude modulated by linear temporal variations of the total input power.

B. INTER-CAVITY MODULATION

1. Zeeman Effect

The Zeeman effect is due to the presence of degenerate energy levels in an atom. Degeneracy occurs when a single energy level contains more than one distinct quantum state, with each state having its own orbital and spin angular momenta. Under normal conditions, when lasing occurs from a degenerate upper energy level to a lower degenerate energy level, a single frequency is emitted. However, under the influence of an external magnetic field, the degenerate quantum levels will separate, or split, into separate energy levels. An individual level may move up or down in energy, depending upon the energy of its dipole magnetic moment's coupling with the external magnetic field. The mean energy of the ensemble of split levels coincide with the original, unsplit degenerate level energy, E_0, as shown in Fig. 2-1.

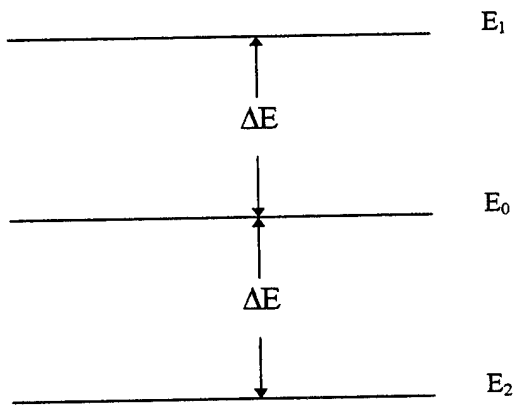

Figure 2-1. Energy level split due to Zeeman Effect.

The split in energy levels results in multiple frequencies being emitted when the electron transitions from an excited level to a lower energy level. The

magnitude of ΔE in Fig. 2-1 is proportional to the strength of the applied magnetic field as (Landau and Lifshitz, 1958),

$$\Delta E = \beta_0 g M_J H \tag{2-1}$$

where H is the strength of the external magnetic field,

$$M_J = -J, -J+1, \ldots, J \tag{2-2}$$

is the projection of the quantum state's total angular momentum along the magnetic field axis,

$$\beta_0 = eh/4\pi mc, \tag{2-3}$$

is the Bohr magneton and,

$$g = 1 + [J(J+1) - L(L+1) + S(S+1)]/2J(J+1), \tag{2-4}$$

is the Landé factor. In Eq. (2-4) L, S and J are the orbital, spin and total angular momentum quantum numbers for the system, respectively. Eq. (2-1) is valid for small H, such that ΔE is much less then the spacing between energy levels of the atom.

2. Theory of Modulation

Using the photon-energy relationship, $\Delta E = h\nu$, Eq. (2-1) becomes

$$\Delta\nu = \frac{eHgM_J}{4\pi mc}, \tag{2-5}$$

for the frequency shift which will occur from the unperturbed frequency emitted during a transition from an excited energy level to a lower energy level. If a DC magnetic field is applied to a lasing medium, frequency shifts, both above and below the unperturbed frequency will occur. If the frequency shift is small compared to the laser cavity gain bandwidth, all frequencies will continue to lase. The simultaneous lasing of multiple coherent frequencies will result in a beating of the frequencies in the cavity. This beating will produce an amplitude modulated output. The pattern of the modulation depends on the orientation of the magnetic field to the laser cavity.

If the cavity is aligned along the same axis as the field and the transition energy levels have doublet or higher structure, the frequency split will be as shown in Fig. 2-2a (Jenkins and White,1976). This is known as the longitudinal Zeeman effect. In this alignment the frequencies $\upsilon_0 + \Delta\upsilon$ and $\upsilon_0 - \Delta\upsilon$ are circularly polarized in opposite directions.

If the field is aligned perpendicularly to the laser cavity, the frequency split will appear as shown in Fig. 2-2b (Jenkins and White, 1976). This is know as the transverse Zeeman effect. In this alignment all three frequencies υ_0,

$\upsilon_0 + \Delta\upsilon$, and $\upsilon_0 - \Delta\upsilon$ are linearly polarized with the sideband frequencies polarized orthogonally to the center frequency.

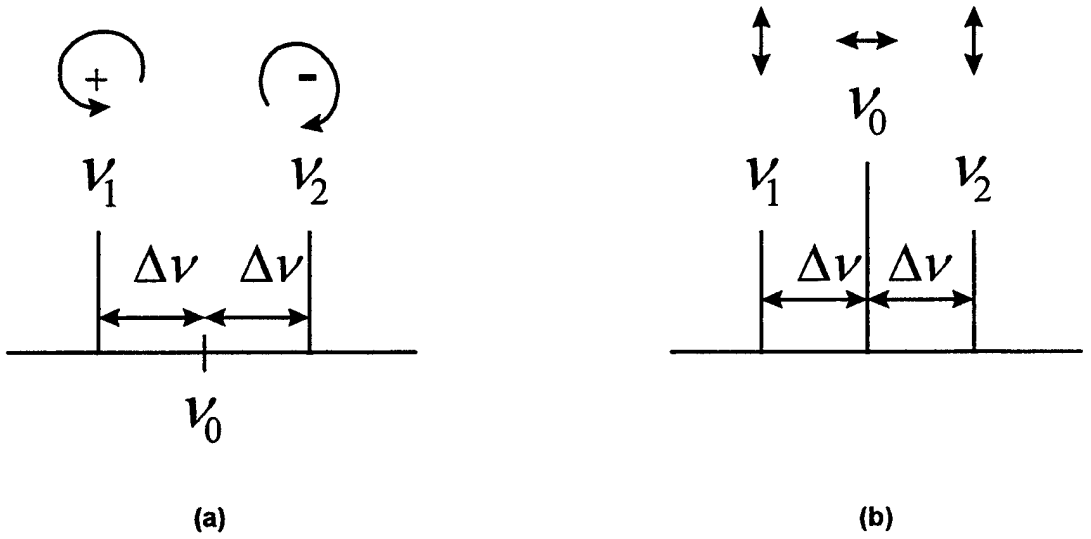

(a) (b)

Figure 2-2. Normal Zeeman effect patterns showing polarization for (a) longitudinal alignment of the magnetic field and (b) transverse alignment of the magnetic field.

From the patterns shown in Fig. 2-2 we see that to obtain a true AM modulation effect, the transverse alignment is required. The patterns depicted in Fig. 2-2 are for a normal triplet. This effect is observed in some spectral lines, but not the majority of them. Many materials exhibit an anomalous Zeeman effect as shown in Fig. 2-3. This is more likely to occur when the energy level is a doublet or higher. These mulitiplet energy levels occur when the total spin quantum number, $S \geq 1/2$. This is also likely when the transition is J-J coupled rather than L-S coupled. In L-S coupling the higher and lower energy levels have well-defined total orbital and spin quantum numbers. In these cases the

Landé factor can be easily calculated. In J-J coupling, the total angular momentum is the only well-defined angular momentum quantum number.

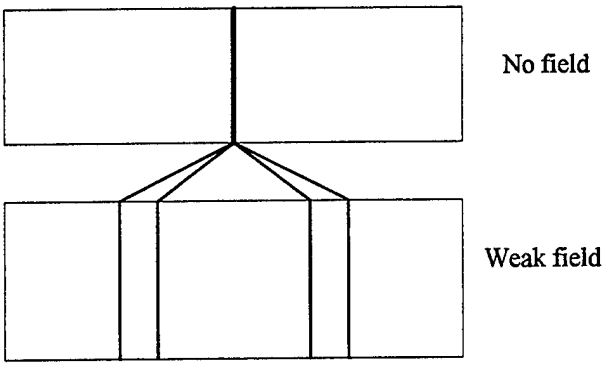

Figure 2-3. Anomalous Zeeman effect for a doublet line.

C. SELF-PHASE MODULATION

1. Nonlinear Optical Loop Mirror

The nonlinear optical loop mirror that we have in mind is shown in Fig. 2-4 (Doran and Wood, 1988). It consists of an optical fiber X-coupler with a power-coupling ratio $\alpha{:}1-\alpha$. In this configuration a single input at port 1, E_{IN}, is split into two counter propagating fields in the loop. Linearly, the optical path length is exactly the same for each field since they travel through the same loop but in opposite directions. The two fields return in coincidence and recombine at the coupler. This design is based on a Sagnac interferometer (Islam, 1994). If the device is maintained in an inertial frame of reference, with an $\alpha = 1/2$, linearly it acts as a perfect mirror providing only constructive interference. Both linear and nonlinear phase differences can be present causing a drift in the fringe pattern. A linear phase difference can be produced by the rotation of the device with

respect to an inertial reference frame. Specifically, a large coil can be effected by the rotation of the earth, creating fringe drifts, as with an optical gyroscope. Due to nonlinearity the paths are no longer identical if $\alpha \neq 1-\alpha$ because, as discussed in Chapter I, the phase velocity is intensity dependent. Thus, for the same length L, two beams of different intensities exhibit a phase difference. The nonlinear phase shift is minor compared to possible linear phase shifts, but can be distinguished if not constant with time, while the linear effects are held constant over time.

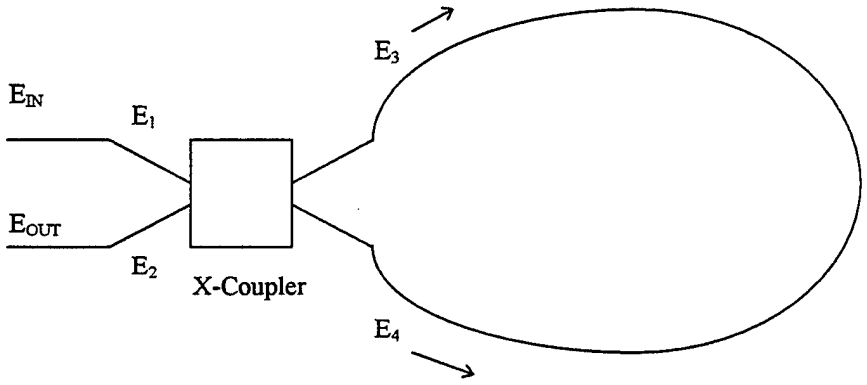

Figure 2-4. Nonlinear-optical loop mirror configuration.

2. Theory of Modulation

The phase of a light wave in a glass fiber, due to nonlinearities, depends on intensity through the relation

$$\phi = \frac{2\pi n_2 |E|^2 L}{\lambda}, \qquad (2\text{-}6)$$

where n_2 is the nonlinear (Kerr) coefficient and L is the physical length of the optical loop.

If the power-coupling ratio at the X-coupler in Fig 2-4 is $\alpha{:}1-\alpha$, for input fields E_1, E_2 at the ports 1 and 2, respectively, the amplitudes of the fields E_3 and E_4 in the loop are given by

$$E_3 = \alpha^{1/2} E_1 + i(1-\alpha)^{1/2} E_2, \tag{2-7a}$$

$$E_4 = i(1-\alpha)^{1/2} E_1 + \alpha^{1/2} E_2. \tag{2-7b}$$

For the simple case where E_{IN} is a single input at port 1, after the fields have traveled around the loop of length L, Eqs. (2-7) become,

$$E_3(L) = \alpha^{1/2} E_{IN} \exp(i\alpha |E_{IN}|^2 2\pi n_2 L / \lambda), \tag{2-8a}$$

$$E_4(L) = i(1-\alpha)^{1/2} E_{IN} \exp[i(1-\alpha)|E_{IN}|^2 2\pi n_2 / \lambda]. \tag{2-8b}$$

Similarly, the amplitude of the fields at the output ports, in terms if the amplitude of the fields in the loop at the coupler is

$$E_1 = \alpha^{1/2} E_4(L) + i(1-\alpha)^{1/2} E_3, \tag{2-9a}$$

$$E_2 = \alpha^{1/2} E_3(L) + i(1-\alpha)^{1/2} E_4. \tag{2-9b}$$

Note that Eqs (2-7), (2-8), and (2-9) are consistent with the limit n_2=0 for which the X coupler acts as a mirror. If E_{OUT} is a single output at port 2, we get

$$E_{\text{OUT}} = \alpha^{1/2} E_3(L) + i(1-\alpha)^{1/2} E_4(L). \tag{2-10}$$

Using Eqs (2-8) and (2-10) the power output at port 2 is,

$$\left|E_{\text{OUT}}\right|^2 = \left|E_{\text{IN}}\right|^2 (1 - 2\alpha(1-\alpha)\{1 + \cos[(1-2\alpha)\left|E_{\text{IN}}\right|^2 \times 2\pi n_2 L / \lambda]\}). \tag{2-11}$$

Thus, for any α≠½, all of the input power $\left|E_{\text{IN}}\right|^2$ is transmitted out at port 2 whenever,

$$n_2 2\pi |E|^2 L / \lambda = m\frac{\pi}{1-2\alpha}, \tag{2-12}$$

for odd *m*. The minimum output power, which occurs for even *m*, is

$$\left|E_{\text{OUT}}\right|^2 = \left|E_{\text{IN}}\right|^2 [1 - 4\alpha(1-\alpha)]. \tag{2-13}$$

The sinusoidal dependence Eq. (2-11) of the output power on the input power leads to a means of amplitude modulating the power of a laser. As the input power is slowly varied linearly, the output varies sinusoidally. The

frequency and magnitude of the modulation are dependent on the parameter α, the intensity of the laser, and the nonlinear properties of the medium. A value of α close to 0.5 will provide the greatest magnitude of modulation, however, a smaller value of α provides a higher frequency.

Figure 2-5 is a plot of the ratio of the output to the input power using Eq. (2-11) for light with a wavelength $\lambda = 1.064\mu m$. The two curves correspond to two different values of α, for the same nonlinear Kerr coefficient $n_2 = 2.8 \text{x} 10^{-15}$ cm^2/W, typical of SF-6 silica glass, and effective fiber cross-section area of $100\mu m^2$. The abscissa of this graph is scaled in units of kilowatt-meters in order to remove the explicit reference to the length of the fiber.

Apparent from the graph is the need to be able to vary the α factor in order to determine experimentally which combination of frequency and magnitude provide the best results for modulation of the laser. Also apparent from the graph is the fact that, in this configuration, the nonlinear optical loop mirror acts as a frequency multiplier modulator. A detailed discussion of the X-coupler design to provide the variable split is provided in Chapter IV.

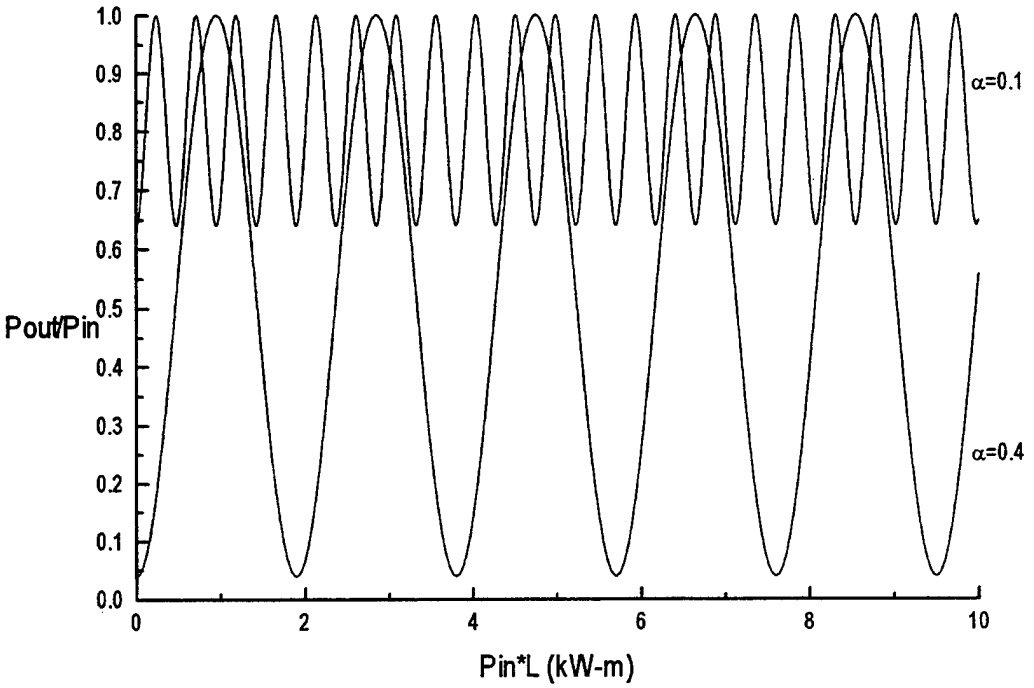

Figure 2-5. X-coupler output to input ratio against input in kilowatt-meters. The lower amplitude curve is for $\alpha = 0.1$ and the larger amplitude curve is for $\alpha = 0.4$.

III. EXPERIMENTAL SETUP AND RESULTS OF INTER-CAVITY MODULATION USING THE ZEEMAN EFFECT

A. OVERVIEW

In order to test the validity of the theories presented in Chapter II, we designed two experiments. In this chapter we report results of inter-cavity modulation using a DC magnetic field to induce a Zeeman effect on a low power helium-neon laser and on an argon ion laser. Both transverse and longitudinal configurations of the magnetic field were investigated.

B. INTER-CAVITY MODULATION WITH ZEEMAN EFFECT

1. Helium-Neon Laser

a. The Helium-Neon Transition

As an initial test of inter-cavity modulation, we applied a magnetic field to a helium-neon laser. This choice of laser was made mainly because of the small size of lasers available which allow fabrication of a solenoid capable of producing magnetic fields up to a kilogauss. The 632.8 nm wavelength transition of the helium-neon laser arises from states that are J-J coupled, and as discussed in Chapter II, this makes the Landé factor difficult to calculate theoretically. In addition, because of the J-J coupling, the anomalous Zeeman effect rather than the normal Zeeman effect is expected to occur.

Figure 3-1 (Harney, 1996) shows the helium-neon energy levels involved in the transition. In this figure the parent electronic configuration is shown at the bottom the graph. The unpaired electron remaining in the unexcited

level has a spin-orbit configuration shown in parentheses as $^{2s+1}l_j$. According to the graph, the unpaired unexcited electron quantum numbers are s=1/2, *l*=1 and *j*=1/2. The excited electron energy level is depicted as nl(j). In all cases, the excited electron has a spin of s=1/2. In the upper energy level, the principal quantum number corresponds to n=5, the orbital momentum is *l*=0 and the total angular momentum for that electron is *j*=1/2. From these conditions the total angular momentum for the system is J= 0 or 1. In the lower energy level, n=3, *l*=1 and *j*=3/2. In this case the total angular momentum for the system is J=1 or 2. In both the upper and lower energy levels, different combinations of orbital momentum, L, and spin momentum, S, can satisfy the selection rules. Therefore, the Landé factor cannot be calculated using Eq. (2-4) directly. Using the various possible combinations of L and S, the Landé factor for the upper energy level is in the range of 1.0 to 1.5. For the lower energy level, the Landé factor is in the range of 1.5 to 2.0.

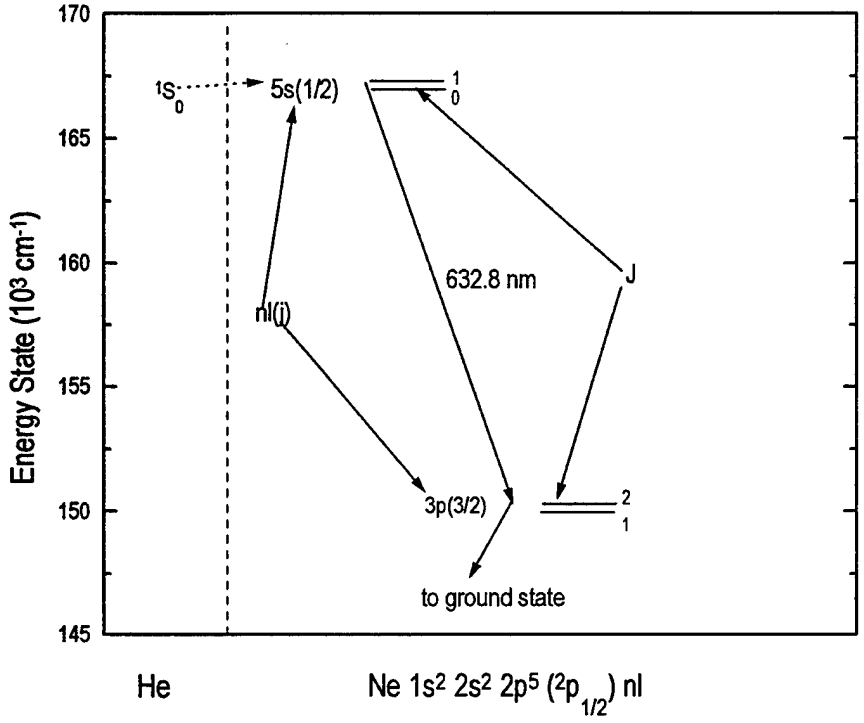

Figure 3-1. Helium-neon transition at 632.8 nm. The traditional spectrographic notation is employed with S, P and D corresponding to the angular momentum quantum numbers L= 0, 1 and 2 respectively.

b. Building a Kilogauss Solenoid

We used two helium-neon lasers, a Hughes 3221H-C 1.1 mW, unpolarized model, and a Uniphase 1101P 4 mW, polarized unit. Both models have a small cylindrical head which can fit in a long, small diameter solenoid. The Hughes laser is 1.75 inches in diameter and the Uniphase is slightly smaller at 1.25 inches in diameter. Both are about 10 inches in length.

A solenoid was used to apply a magnetic field to the helium-neon lasers. The dimensions of the solenoid, 2 inches inner diameter and

approximately 12 inches long, were chosen to fit both laser models. The solenoid was made by coiling 14 gauge copper wire around a PVC pipe core. For a solenoid, the on-axis near-center magnetic field strength, *H,* is

$$H = \mu_0 in, \qquad (3\text{-}1)$$

where μ_0 is the permeability constant, *i* is the DC current through the solenoid coil and *n* is the number of turns per unit length. We wanted to generate a maximum field of 0.1 tesla Thus, according to Eq (3-1), for a maximum DC current of 10 A, 1 kgauss (0.1 tesla) corresponds to n=7957.7 turns/m. For the a solenoid 12 inches long, 13 layers of coils were required. Fig. 3-2 shows a photograph of both lasers and of the solenoid.

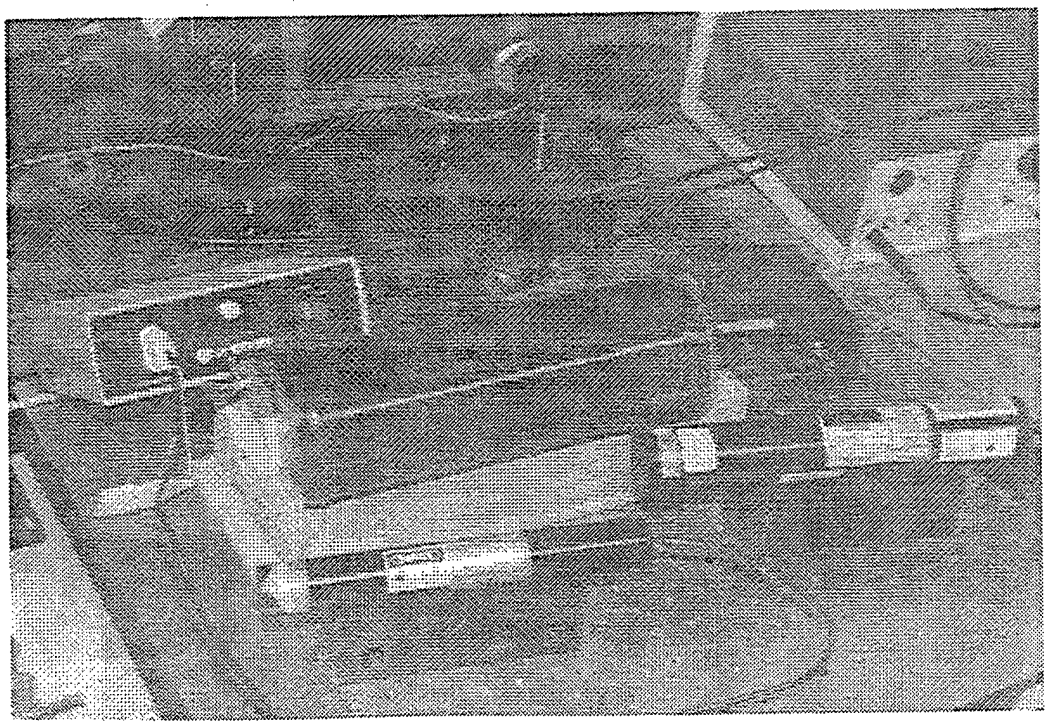

Figure 3-2. Photograph showing the 1 kilogauss solenoid with the 1.1 mW Hughes helium-neon laser and the 4 mW Uniphase helium-neon laser.

The DC resistance of the solenoid was measured to be 5.0 ohms, requiring a 50 volt power supply to produce the 10 A desired. An HP 6274B DC power supply with a range of 0-60 V at 0-15 A was used to deliver the appropriate current. However, ohmic heating prevented long-term use of the solenoid above 5 A. Fig. 3-3 shows a plot of the magnetic field strength, measured near the center of the solenoid, as a function of the DC current. The magnetic field was measured using a RFL Industries Inc. model 912 guassmeter. As predicted, a linear relation between the magnetic field and the current is apparent. The measured field strength is approximately 10% less than that predicted by Eq. (3-1) probably due mainly to fringe effects.

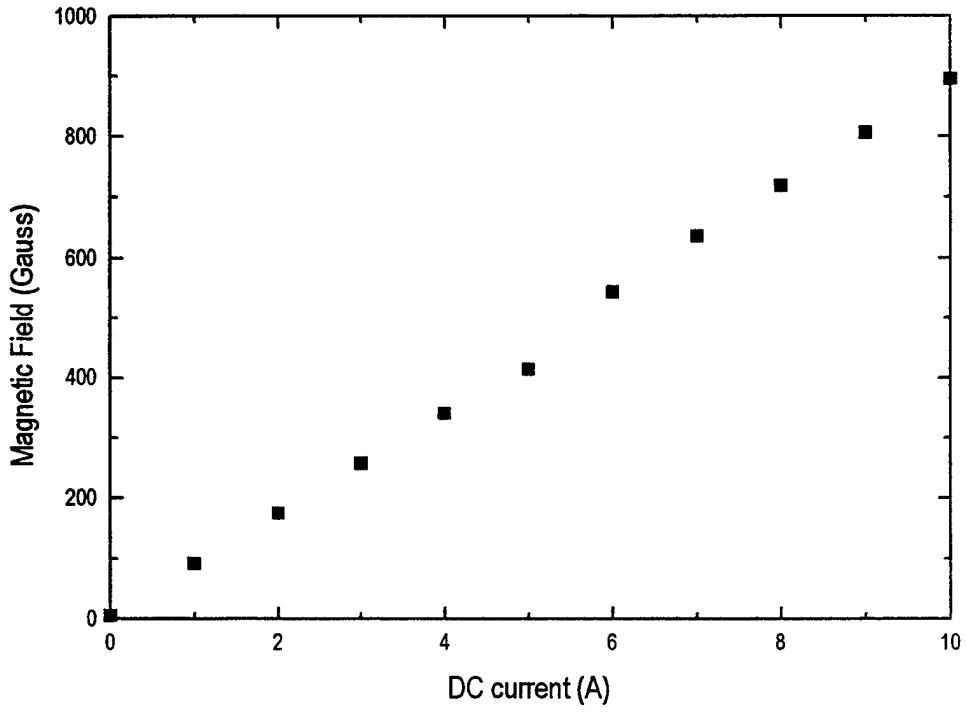

Figure 3-3. Magnetic field produced in solenoid as a function of DC current.

c. Search for Modulation

Initially, we attempted to observe the modulation using a Opto-Electronic PD30 Series Ultra High-Speed Photodetector made with an avalanche silicon photodiode. The PD30 has a specified optical response bandwidth of 1 GHz and a measured response in the lab of greater than 250 MHz. The output of the PD30 was DC coupled to a Tektronix 7104 analog oscilloscope which has a maximum frequency response of 2 GHz. When the Hughes laser was mounted inside the solenoid, broadening of the oscilloscope DC line was observed at a current of approximately 1.2 A, corresponding to a magnetic field of about 105 gauss. No other effect was noted for any other current up to 10 A.

We measured the laser line spectrum under the influence of the magnetic field using a Tropel 360 Fabry-Perot interferometer and a Tropel 361 Fabry-Perot controller. The etalon of the Fabry-Perot interferometer produces sharp fringes due to multiple beam interference pattern. For each mode, a separate fringe pattern is produced. As the distance between the etalon's plates is increased, sequential frequency fringes are generated. If the plates are moved far enough, the fringe pattern will repeat for each frequency. The spacing between like fringes, corresponding to consecutive spectral orders, is related to the etalon spacing as,

$$FSR = \frac{c}{2nd}, \qquad (3\text{-}2)$$

where FSR stands for free spectral range measured in frequency, c is the speed of light in air, n is the index of refraction in air, and d is the etalon spacing. In all cases we used $c = 3 \times 10^8 \, m/s$ and n = 1.0.

Baseline observations were made for both the Hughes and the Uniphase helium-neon lasers without the solenoid. These measurements were taken using a Newport 818-SL silicon diode photodetector connected to a Newport 815 series power meter. The analog output of the power meter was connected to a HP 35670A dynamic signal analyzer. The spectrum of the Hughes laser is shown in Fig. 3-4, and the Uniphase spectrum appears in Fig. 3-5. The scan rate for the etalon was 2 Hz. The abscissa is the time measurement of the etalon scan. Using Eq. (3-2), the time scale is converted to frequency scale. The etalon spacing was d=2.5 cm for both spectra, which corresponds to a FSR of 6 GHz. From these spectra, it is clear that neither helium-neon laser was operating in single mode. The gain curve for each laser is about 5 GHz wide. Due to the wide gain curves, both lasers exhibit multiple longitudinal mode structure under the gain curve. The spacing between adjacent modes of the laser is related to the length of the laser cavity by Eq. (3-2). In this case the FSR is equal to the spacing between modes and d is the length of the laser cavity. Based on the absence of single longitudinal mode structure we determined that the helium-neon lasers were not good potential candidates for observing Zeeman-induced AM modulation. This is due to the fact that there are numerous, closely spaced longitudinal modes under the gain curve. Furthermore, any small frequency shifts in the individual modes, such as

those caused by slight thermal changes in the laser resonator's length, would blur by an adjacent modes together in a dynamic and uncontrollable fashion.

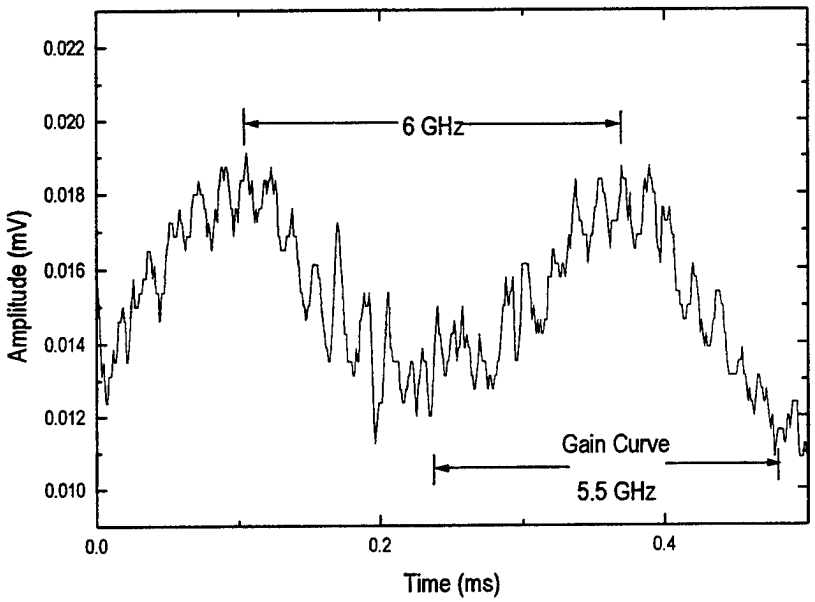

Figure 3-4. Hughes 1.1 mW helium-neon laser spectrum without solenoid.

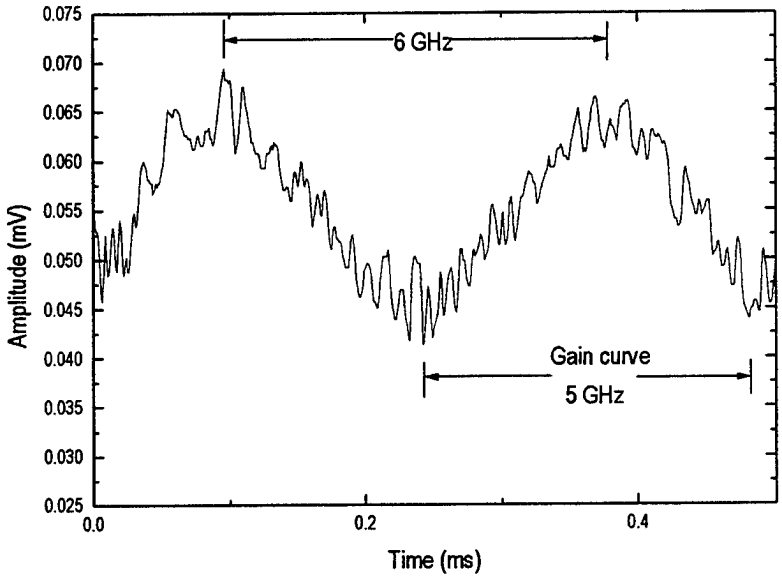

Figure 3-5. Uniphase 4 mW helium-neon laser spectrum without solenoid.

Figs. 3-6 and 3-7 show the spectrum of Hughes laser and the Uniphase laser, respectively for 0A, 3A, 6A, 10A DC currents through the solenoid. The FSR is the same as in Figs. 3-4 and 3-5. The etalon scan rate is again 2 Hz. In both of these figures, individual mode line splitting cannot be discerned. The overall effect in both cases is a detuning of the laser, resulting in lower power output. In order to further study the Zeeman effect in the helium-neon lasing line a single mode laser would have to be used. A single mode laser would allow a larger etalon spacing which would improve the resolution of the laser spectrum.

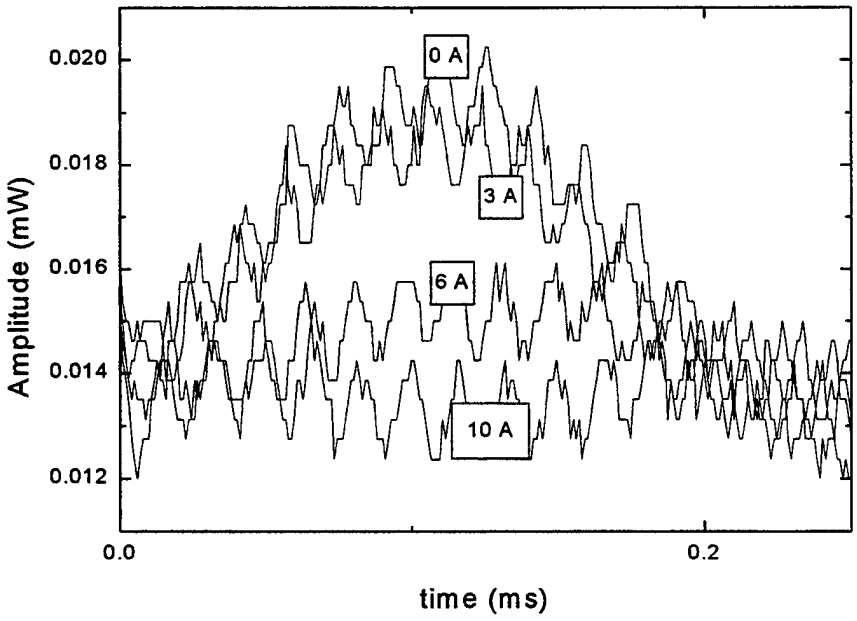

Figure 3-6. Hughes 1.1 mW helium-neon spectrum in a solenoid. Note the decrease in power output as the current is increased for currents of 0A, 3A, 6A, and 10A.

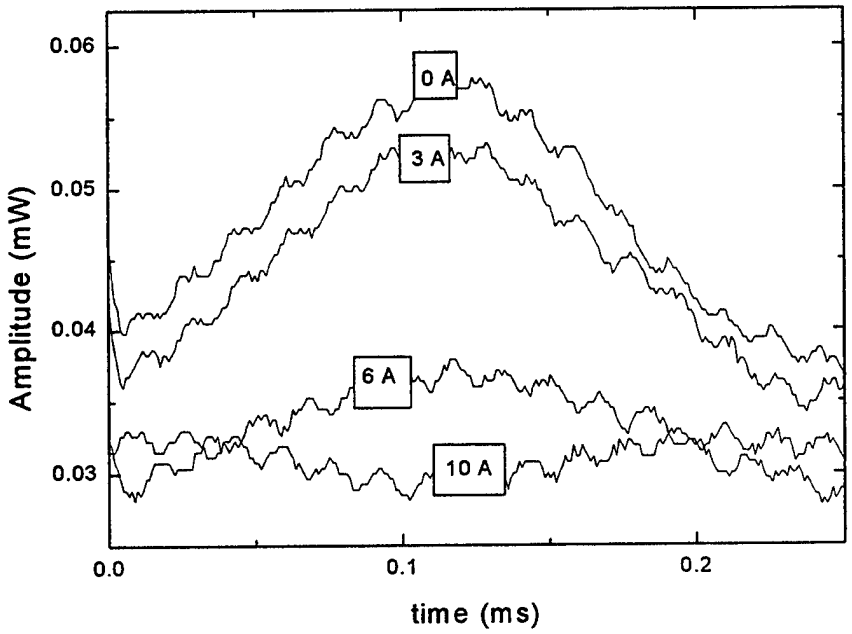

Figure 3-7. Uniphase 4 mW helium-neon laser spectrum in solenoid. As in Fig 3-6, power output decreases as the current is increased for currents of 0A, 3A, 6A, and 10A.

2. Argon Ion Laser

a. The Argon Ion Transition

A second choice of laser for observing the Zeeman effect was an argon ion laser. The argon ion laser 514.5 nm transition is shown in Fig. 3-8 (Harney, 1996). The relevant quantum states are L-S coupled, making the Landé factor calculation simple. The electronic levels are shown in conventional L-S notation. For the upper level S=3/2, L=2 and J=5/2. Using Eq. (2-4) the Landé factor for this level is 1.3714. In the lower level S=1/2, L=1 and J=3/2. The Landé factor for this level is 1.3333. The upper and lower excited states for this transition are multiplets. This indicates that anomalous, rather than normal Zeeman splitting should occur, but is less likely than with the helium-neon laser.

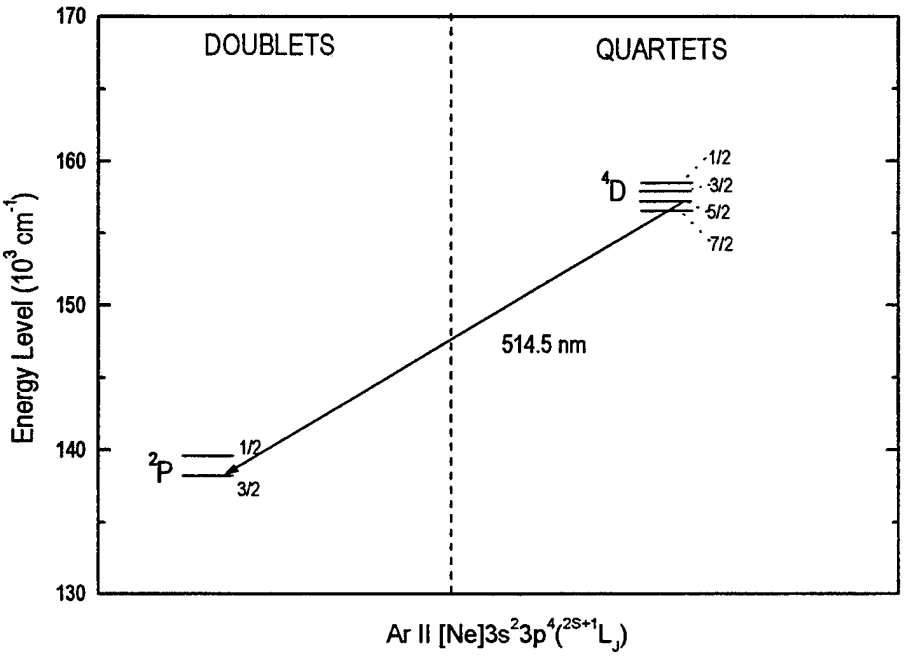

Figure 3-8. Argon ion laser transition at 514.5 nm.

b. Helmholtz Coils

The argon ion laser used for this experiment is a Lexel 85 Series CW Laser. The Lexel laser can operate in either multi-mode or single mode, with a maximum output power of 300 mW in the single mode configuration. The outside dimensions of the laser case are 5 inches high by 7 inches wide by 34 inches long. This large case size made it difficult to fabricate a high field strength solenoid as was done for the helium-neon laser. Instead, large diameter Helmholtz coils were used.

Helmholtz coils (Fig 3-9) consist of two circular coaxial coils each of N turns and radius R, separated by a distance R. The two coils carry equal

currents in the same direction. For this configuration, the field between the coils is uniform in the vicinity of the center of the common axis.

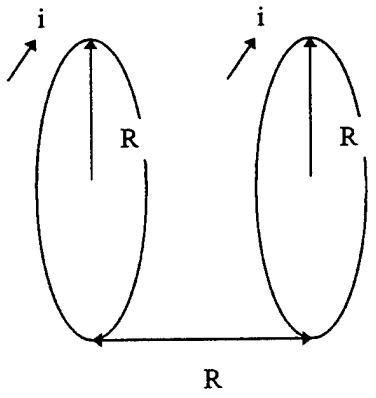

Figure 3-9. Helmholtz coils arrangement.

The coils used were 12.5 inches in diameter, making the optimum inter-coil separation distance 6.25 inches. The coils were wound from multiple layer 18 gauge copper wire with a non-magnetic core. The total DC resistance of the coils, when connected in series, was 25.5 ohms. Due to the smaller gauge wire, these coils would be limited to a lower maximum operating current than was the case for the solenoid built for the helium-neon laser experiments. A current of 3.5 A would require a 90 volt DC current supply. To achieve this an HP 6274B DC power supply (0-60 V at 0-15 A) was connected in series with an HP 6434B DC power supply (0-40 V at 0-25 A). This arrangement was able to provide up to 100 V.

Off of the common axis, the magnetic field is not uniform. Figure 3-10 shows the relationship between DC current and magnetic field for the nine

locations indicated on Fig. 3-11. The magnetic field was measured using the RFL guassmeter. From the data we can see that the field is uniform along the common axis at points 1, 2, and 3. This field is about 50% of the of the maximum field seen at the outer edge of the coils at points 4, 6, 7 and 9. The field at the top and bottom circumference of the coil diameter on the center line between the coils at points 5 and 8 is about 60% of the on axis uniform field. The uniformity of the on axis field was consistent within 10% out to approximately 2/3 of the radius of the coils.

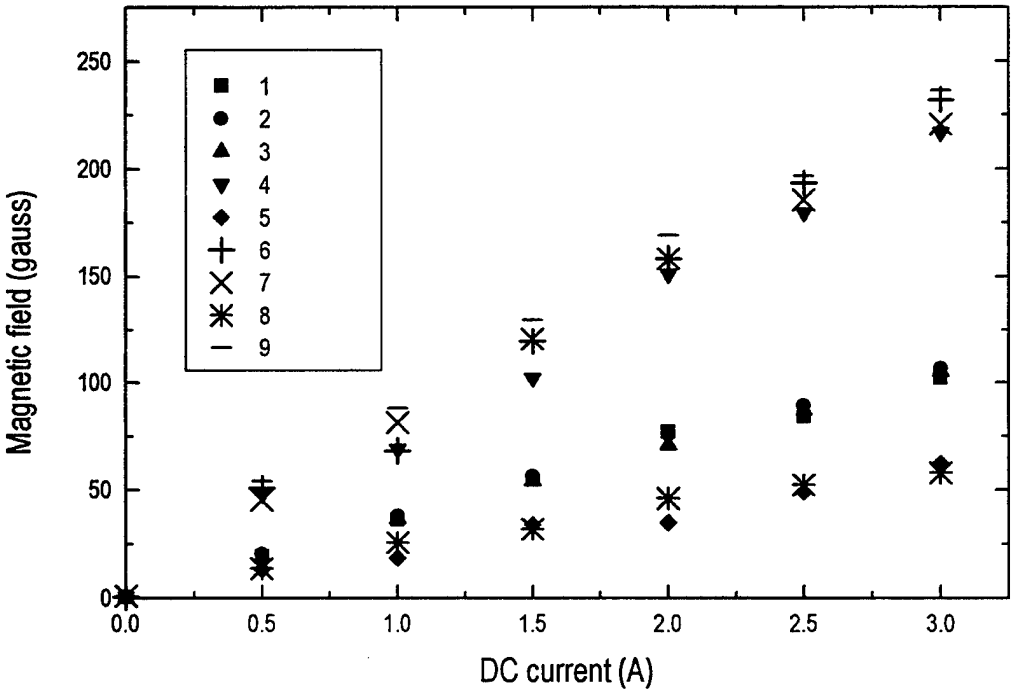

Figure 3-10. Magnetic Field produced at various points of the Helmholtz coils configuration. Points indicated correspond to points shown in Fig. 3-11.

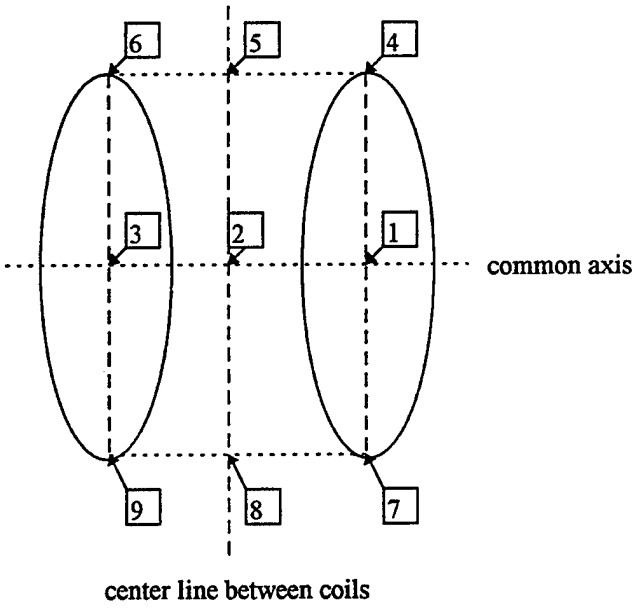

Figure 3-11. The numbers show the locations where the magnetic field was measurement as plotted in Fig. 3-10.

c. Transverse Configuration

The main advantage of using the Helmholtz coils is that both longitudinal and transverse Zeeman effect can be investigated. Fig. 3-12 shows the coils and the Lexel laser in the transverse configuration. In this configuration, the coils had to be separated by 9.5 inches due the width of the laser case. In addition the Lexel laser active medium case is not centered in the laser case. It is located, as shown in Fig. 3-13, on the left side of the case when viewed from the back end of the laser. This configuration resulted in a magnetic field applied to the active medium case as shown in Fig. 3-14 at points indicated in Fig. 3-15. The magnetic field was measured using the RFL guassmeter. From these figures we note that the field is uniform longitudinally along each

side of the active medium, but experiences a drop perpendicularly across the active medium case. The drop ranged from 41% at 0.5 A down to 27% for currents above 2.0 A. This variation is due to the fact that the separation of the coils is greater than the optimum and the case was situated one inch above the center line of the coils. The longitudinal variation on the inner side of the case is due to the fact that the length of the case is about ¾ of the diameter of the coils. This caused the end of the case to be at the edge of the uniform field at that point between the coils.

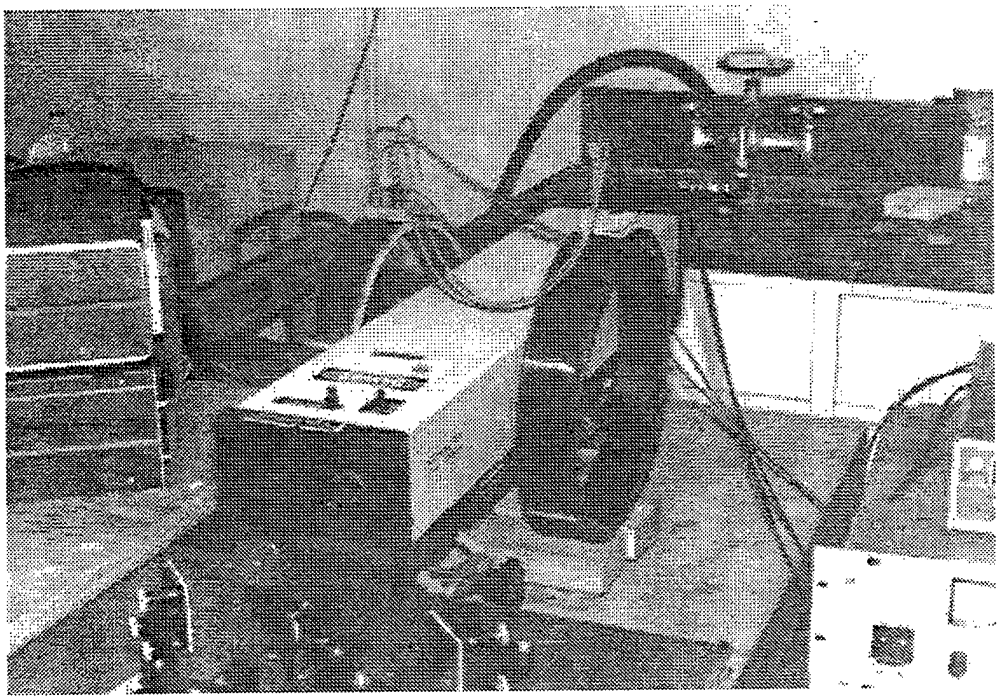

Figure 3-12. Photograph of the Lexel argon laser with the Helmholtz coils arranged in the transverse configuration.

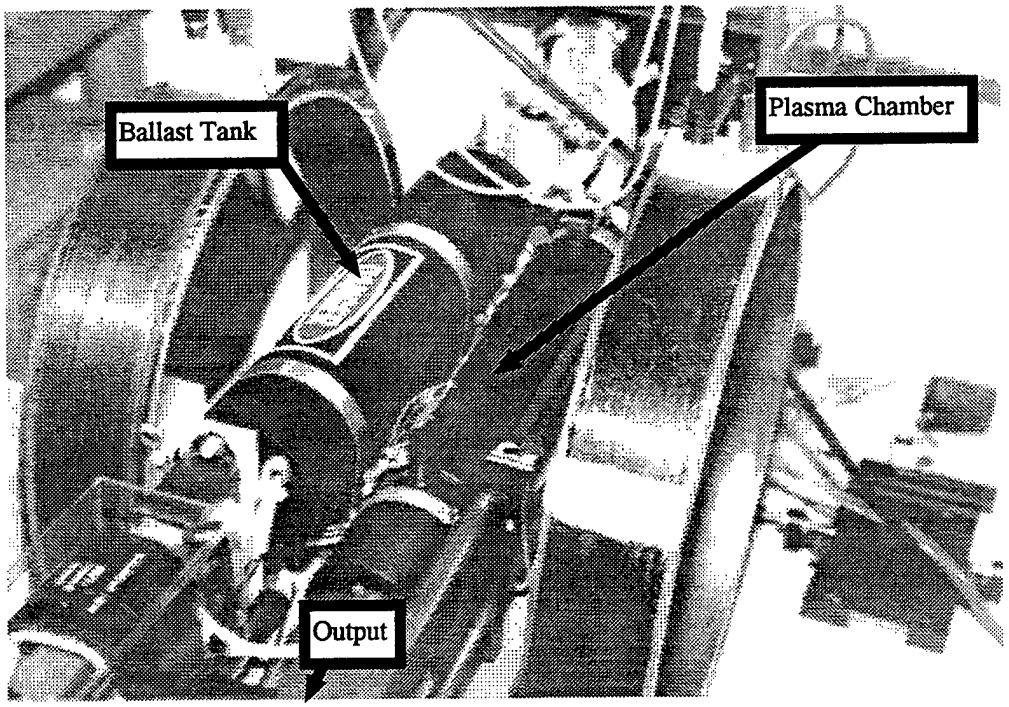

Figure 3-13. Plasma chamber arrangement in the Lexel argon ion laser. Plasma chamber is on the right side of the laser case when viewed from the rear of the laser.

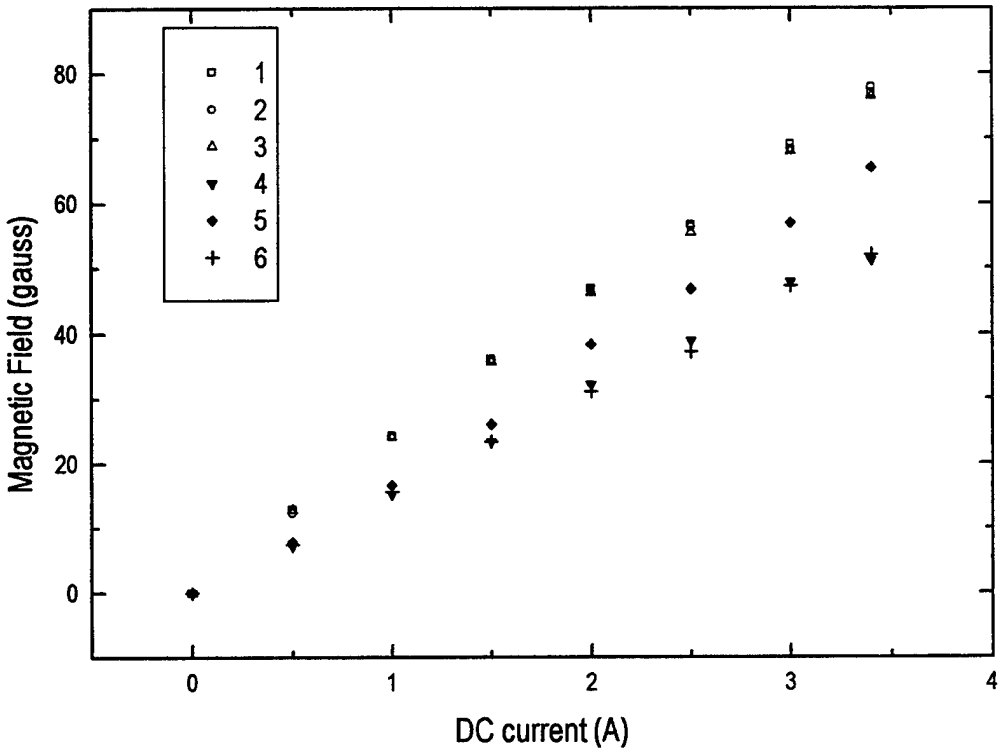

Figure 3-14. Magnetic field applied to the argon ion laser plasma chamber in the transverse configuration. Measurement locations indicated refer to the locations indicated in Fig. 3-15.

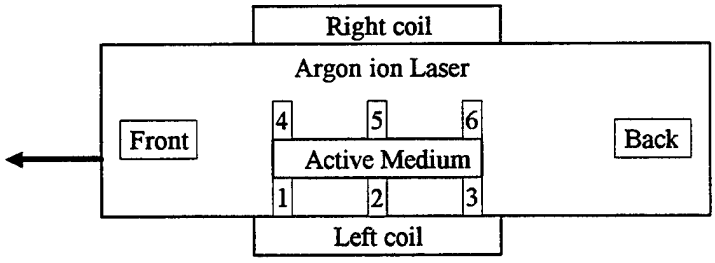

Figure 3-15. Magnetic field measurement locations in the transverse configuration. The same locations were used when making measurements in the longitudinal configuration (See Fig. 3-17).

d. Longitudinal Configuration

An experiment was also conducted using the Helmholtz coils in the longitudinal configuration on the argon ion laser. Figure 3-16 shows the laser and the coils in this configuration. In this configuration the coils could now be placed at the optimum spacing of 6.25 inches to provide a uniform field along the common axis. The length of the active medium chamber is approximately 9 inches, causing the chamber to extend slightly beyond the end of the uniform field produced by the coils.

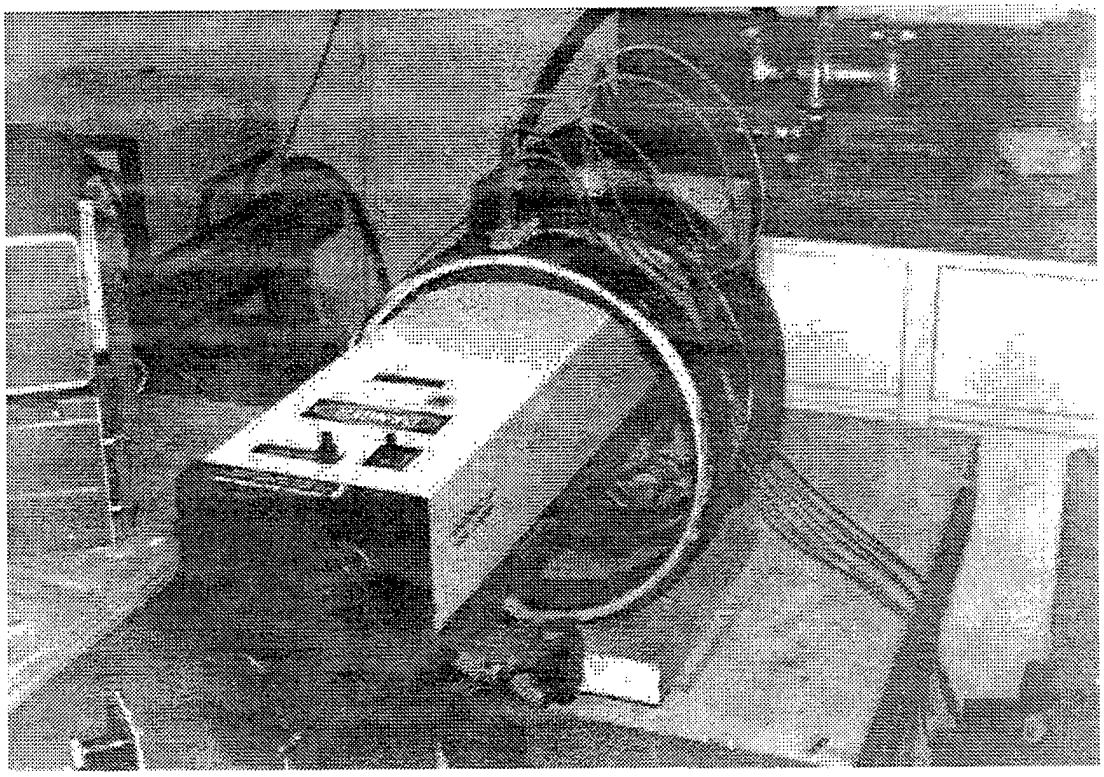

Figure 3-16. Photograph showing the Lexel argon laser and the Helmholtz coils in the longitudinal configuration

The resulting magnetic field produced by the Helmholtz coils in this configuration is shown in Fig. 3-17, which indicates the field at the locations

indicated in Fig. 3-15. The magnetic field was again measured using the RFL guassmeter. As can be seen by this graph, the field is more uniform around the cavity than was achieved in the transverse configuration.

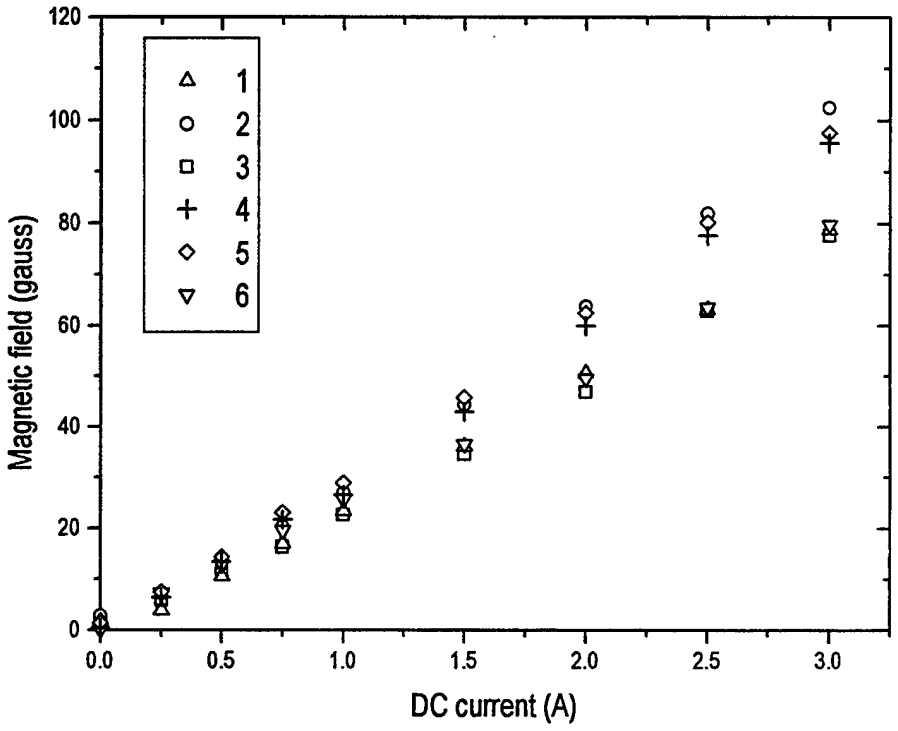

Figure 3-17. Magnetic field applied to the argon ion laser plasma chamber in the longitudinal configuration. The numbered locations refer to locations indicated in Fig. 3-15.

e. Search for Modulation

As with the helium-neon laser, an initial attempt to observe a modulation was made with the argon laser operating at 2 mW power in the transverse configuration. We again used the Opto-Electronics high speed PD-30 detector and the 2GHz Tektronix analog oscilloscope. The low power of the laser was necessary due to the limited power capability of the PD-30 detector. The result was similar to those we saw with the helium-neon laser. A slight

broadening of the line was observed with coil currents below 1A, and then the DC line became much thinner as the current approached 3.5 A. No direct modulation was noted at this laser power.

We next attempted to observe the Zeeman splitting of the argon laser spectrum using the Fabry-Perot interferometer. For this experiment the etalon spacing was increased to 10 cm. This spacing reduced the FSR to 1.5 GHz which increased the resolution of the spectrum by factor of 4 over that in the helium-neon experiment. Fig. 3-18 shows the Lexel argon ion laser spectrum without any external field applied to the laser. The etalon scan rate was 1 Hz.

Figure 3-19 shows the resulting spectrum with a 3.5 A DC current applied to the Helmholtz coils in this configuration. Using the FSR of 1.5 GHz, the frequency shift between the Zeeman split spectral lines are 170 MHz and 125 MHz as shown in the figure. From Fig. 3-14 we find that the magnetic field applied to the active medium at this current is in the range of 77 to 52 gauss with a 66 gauss nominal value. Using Eq. (2-4) and the Landé values calculated earlier, we find the that upper energy level in the argon transition would experience a 316 MHz shift. The lower energy level would experience a 184 MHz shift. Four sets of lasing lines are possible if both the upper and lower energy levels are split. Figure 3-20 shows the four possible lines and the combination of the frequency shifts which produce them. Lines 1 and 2 occur with a total shift of upper shift plus the lower shift. This would give a frequency shift of 500 MHz, which was not observed. The other two frequency lines are a

result of the difference between the upper and lower frequency shifts. This would give a frequency shift of 184 MHz which closely coincides with the frequencies observed in Fig. 3-19. The length of the Lexel laser cavity is 0.8m (Lexel Laser Inc., 1996) which would produce mode lines separated by 188 MHz using Eq. (3-2).

The split was unstable as indicated by the difference in the two consecutive spectra. The instability of the split spectrum is suspected to be due to a combination of three causes. The first and most difficult to correct is the interaction between the induced magnetic field in the transverse direction and the permanent magnetic field required in all argon ion lasers in the longitudinal direction to keep the electrons in the plasma field away from the chamber wall (Silfvast, 1996). The strength of the permanent magnetic field is unknown since it is induced electro-magnetically when the laser is in operation (Lexel Laser Inc., 1996). The second and most dramatic cause was the internal etalon in the Lexel laser which provided the single mode characteristics. When these data were recorded the laser was de-tuned slightly so that the laser produced more than one longitudinal mode. This process was very difficult to reproduce due to extreme tuning sensitivity of the laser resonator. The third cause is the lack of a completely uniform magnetic field as described above. The split did, however, appear consistently as a triplet of spectral lines. This indicates that the argon laser is a good candidate for achieving true AM modulation, if its the spectrum can be stabilized for a sufficiently long period.

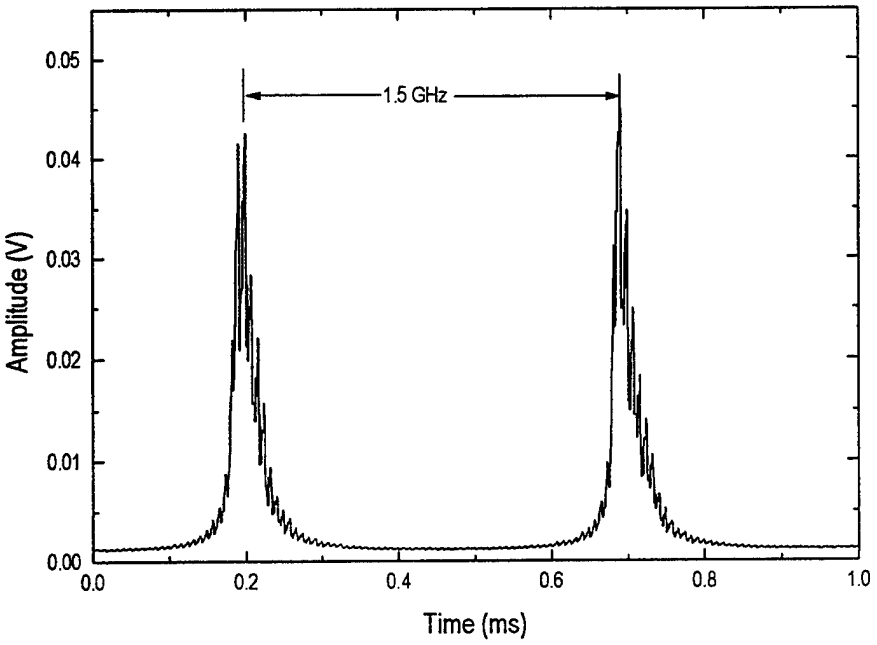

Figure 3-18. Argon ion laser spectrum with no magnetic field applied. The FSR is 1.5 GHz for a Fabry-Perot interferometer etalon spacing of 10 cm.

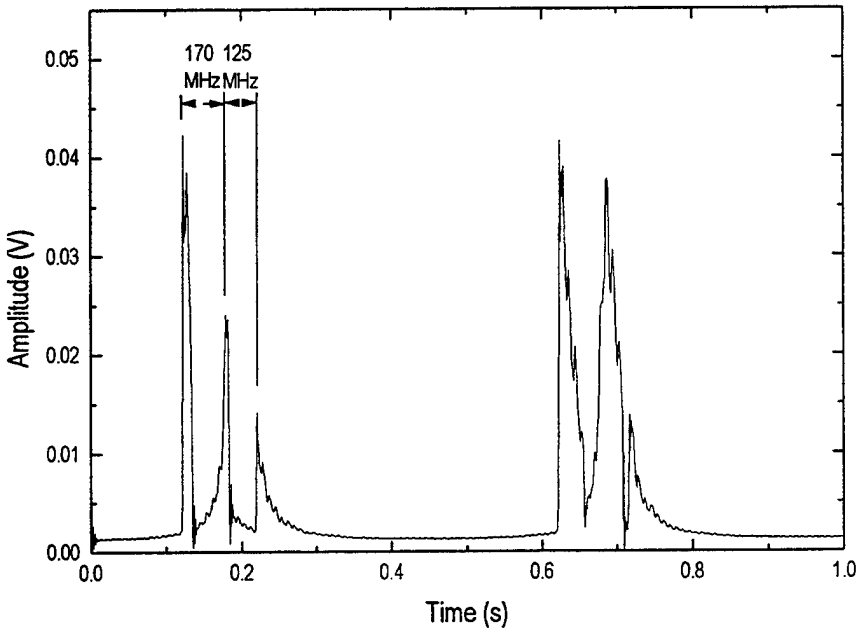

Figure 3-19. Argon ion laser spectrum with a nominal 66 gauss magnetic field applied in a transverse configuration. The FSR is the same as in Fig. 3-18.

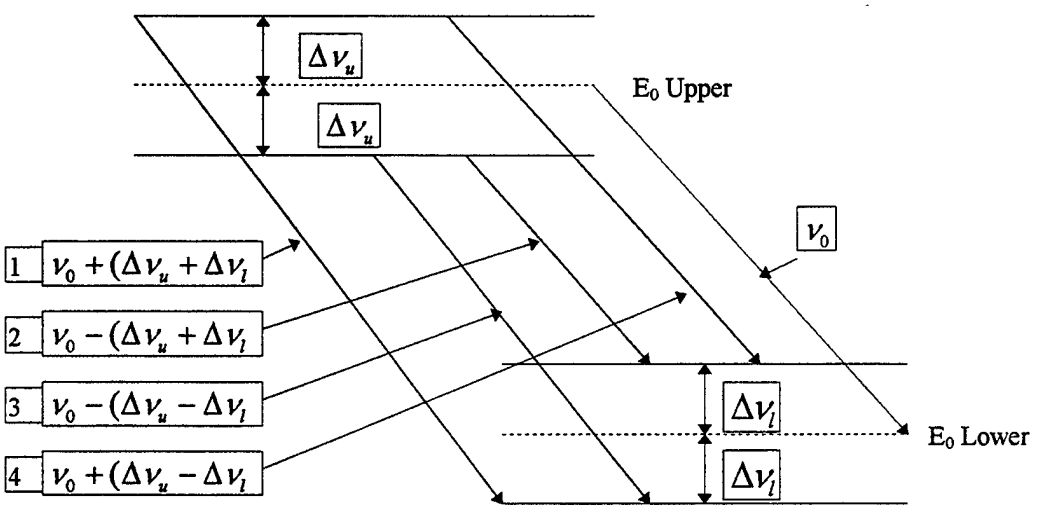

Figure 3-20. Possible Zeeman split lasing lines assuming a Normal Zeeman split. Lines 1 and 2 will act as a pair of sidebands at a high frequency. Lines 3 and 4 act as lower frequency pair of sidebands.

An experiment conducted with the Helmholtz coils arranged in the longitudinal direction also resulted in the production Zeeman split sidebands. Figure 3-21 shows the base line spectrum for this experiment. The Fabry-Perot interferometer etalon spacing was again 10 cm, giving a FSR of 1.5 GHz. The scan rate was increased to 5 Hz. The laser was again slightly de-tuned to allow the additional longitudinal modes to lase. In the base line spectrum a longitudinal mode that differs from the primary mode by 3 orders can be seen. It is not clear why the other modes between the third mode and the primary lasing mode do not appear. Figure 3-22 shows the argon spectrum with 0.25 A current applied to the Helmholtz coils, causing a magnetic field in the aft to fore direction. From Fig. 3-17 we see that this equates to a magnetic field of nominally 6 gauss being applied to the plasma chamber. The split is measured at 214 MHz, which again closely coincides with the single mode spacing of 188

MHz. When the current in the coils was reversed, producing a fore to aft magnetic field, the same split occurred with 0.5 A applied. This indicates that the permanent magnetic field of the laser is arranged in an aft to fore direction. In this configuration the Zeeman split was much more stable over time. This indicates that the induced magnetic field - permanent magnetic field interaction and/or the lack of a uniform magnetic field caused the majority of the instability seen in the transverse configuration.

Of particular note is the continued presence of the original frequency line in the longitudinal Zeeman split. Theoretically this was not supposed to occur. This is an indication that not all of the atoms in the plasma chamber were being split with this magnetic field applied. This situation could still lead to a true AM modulation even in the longitudinal configuration. In addition the percentage of modulation could be controlled.

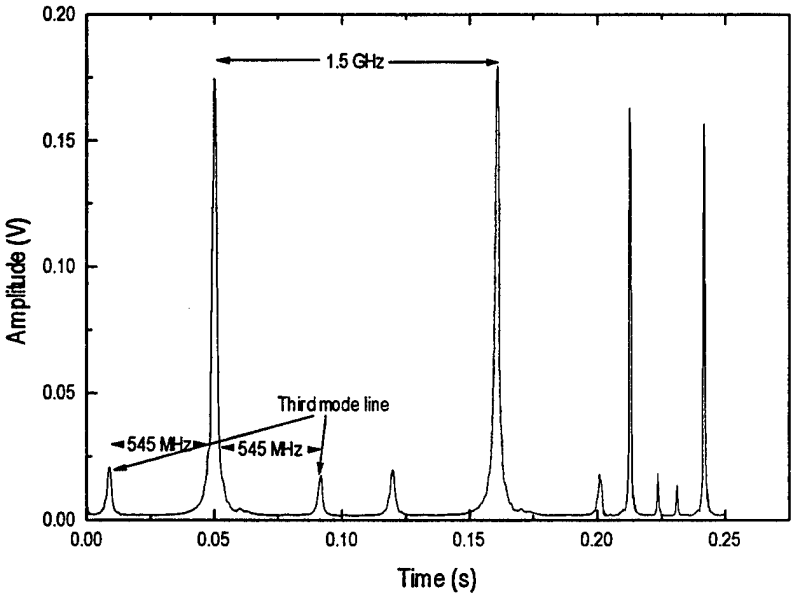

Figure 3-21. Base line spectrum of the argon ion laser. FSR = 1.5 GHz for a Fabry-Perot interferometer etalon spacing of 10 cm. Laser de-tuned to show extra mode lines.

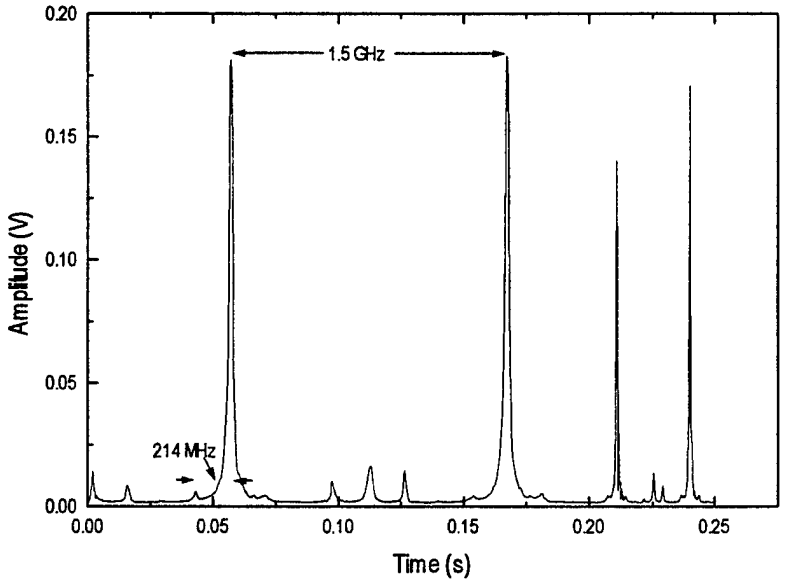

Figure 3-22. Argon ion laser spectrum with the cavity de-tuned to show additional modes and a 6 gauss magnetic field applied in line with the permanent magnetic field.

IV. CONCLUSIONS AND FUTURE WORK

A. CONCLUSIONS

This thesis presented two designs for modulation which do not require electro-optical devices. In the first, we proposed to use the Zeeman effect to induce splitting of the energy levels of atoms in the active medium of a laser. The mutual interference of the multiple frequencies would cause a beating effect leading to modulation. We called this type of modulation inter-cavity, because the modulation occurs inside the laser cavity.

Experiments using a strong magnetic field oriented parallel to the cavity axes of two helium-neon lasers were inconclusive due to the multiple mode structure and thermal instability of the lasers. When Zeeman split, the spectra were smeared out by the nearby adjacent modes, and varied rapidly due to thermal fluctuations of the resonator cavities.

We also conducted experiments using Helmholtz coils, which provided a weaker magnetic field, on a Lexel 85 argon ion laser. The distance between lasing modes for the Lexel laser was 187.5 MHz. With the Helmholtz coils both transverse and longitudinal orientations of the magnetic field were investigated. We succeeded in observing a frequency split of the 514.5 nm line in the argon ion laser in both the transverse and longitudinal configurations of the magnetic field using a Fabry-Perot interferometer.

In the transverse configuration the frequency shift observed appeared as a normal Zeeman pattern, with a central frequency and two sidebands. The

magnitude of the frequency shift corresponded to the difference in the energy split of the upper and lower energies in the lasing transition. The frequency shift observed was unstable with time. We suspect that the unstable nature of the spectrum is due to the permanent low level longitudinal magnetic field required in an argon laser to stabilize the electron flow. In addition, the instability may be due to the lack of a completely uniform magnetic field. The non-uniform magnetic field was caused by the small diameter of the Helmholtz coils compared to the length of the active medium chamber. The frequency split was in the range of 125 to 180 MHz coinciding with one longitudinal mode spacing of the laser cavity.

In the longitudinal configuration a more stable frequency split was observed. The frequency shift did not match the theoretical split into separate frequencies. The original frequency line remained, due possibly to incomplete splitting of all atoms in the active medium chamber because the applied magnetic field did not uniformly extend the full length of the chamber. The frequency split was 214 MHz, again coinciding with one longitudinal mode spacing of the laser cavity. The instability observed in the transverse configuration was not present because the induced field was parallel with the laser's permanent field rather than perpendicular to it.

The permanent magnetic field required for the operation of the argon laser leads to problems in producing a stable frequency split in the transverse configuration. The longitudinal configuration is more stable, but theoretically will not give a true AM modulation spectrum. We may, however, be able to use the

observed lack of complete splitting of all atoms to produce all three required frequencies in this configuration. The fraction of atoms with split energy levels would have to be adjusted to produce a larger percent modulation than observed in these experiments.

Another problem which existed in the Lexel argon laser used in our experiments was the inability to see additional modes appear due to the internal etalon in the laser. A laser without this etalon, but still having a narrow gain curve allowing only 3 to 5 modes would be useful in seeing the Zeeman split more carefully.

The Zeeman frequency shift which will lase is theoretically limited by the width of the gain curve and must coincide with a resonance frequency of the laser's cavity length, which is fixed. Therefore, this method of modulation, while showing promise for a non-electro-optic method, does appear to have limitations in the number and magnitude of available modulation frequencies.

In the second design, a nonlinear optical loop mirror is proposed as a means to induce modulation in a single optical fiber due to nonlinear self-modulation effects. This method should work as a frequency multiplier. A relatively low frequency modulation in the 100s of kHz range could be multiplied by up to 4 orders of magnitude to achieve GHz output modulation. This method would require a highly doped fiber with a Kerr coefficient of 10^{-11} cm^2/W or higher. This is a similar value of the Kerr coefficient need to produce the AM-FM conversion in reasonable lengths of fiber. Fibers with this high value of Kerr coefficient have been achieved, but technology does not currently exist to

reproduce them on a consistent basis. In addition a means of varying the ratio of the split of the laser input into each end of the fiber is needed.

B. FUTURE WORK

1. Inter-Cavity Modulation

In order to fully explore the capabilities of the inter-cavity modulation, more experiments should be conducted using a large cross-sectional area uniform magnetic field on a stable single mode argon laser such as the Lexel laser used in the experiments in this thesis. Additional laser sources such as Nd:YAG and solid state lasers should also be explored. A laser with a wide enough gain curve to excite additional modes with large mode spacing would provide the highest modulation using this method.

2. Self-Modulation

a. Building a Variable X-Coupler

A key element of providing experimental results for the self-modulation theory is a variable X-coupler. Since most commercially available X-couplers are either 50:50 ratio or other fixed ratio, we found necessary to design our own variable X-coupler. The X-coupler uses an internal reflection attenuator as its basis. The attenuator consists of two 90^0 prisms with the 45^0 sides in close proximity as shown in Fig. 4-1. For a single prism the index of refraction is such that a 45^0 incidence is greater than the critical angle, θ_c, given by,

$$\theta_c = \sin^{-1}(\frac{n_2}{n_1}), \qquad (4\text{-}1)$$

where n_1 is the index of refraction for the prism and n_2 is the index of refraction of the medium surrounding the prism. The medium surrounding the prism is normally air, so that $n_2 \approx 1.0$.

An evanescent wave extends beyond the reflecting surface of the prism. The evanescent wave decays exponentially with distance from the prism-air interface with an attenuation length, δ, which is normally on the order of the wavelength of the light. If another medium with a similar index of refraction to the first medium is placed a few units of δ away from the first medium, the evanescent wave will transmit into the third medium. If the first and third medium are identical, as in the case of two 90^0 prisms, an n_1-n_2-n_1 sandwich can be formed. (Guenther, 1990) In this configuration, shown in Fig. 4-1, a fraction, α, of the input light into the first prism will be transmitted into the second prism in the initial direction. The remainder of the light which is not transmitted, $1-\alpha$, is reflected off the 45^0 interface of the first prism and sent out at a 90^0 angle to the input.

This configuration is called a frustrated total internal reflection (FTIR) attenuator. The fraction of transmitted power is now variable because the fraction, α, is dependent on the spacing, d, between the two prisms. Since the evanescent wave intensity drops off as an exponential, we expect the change in α to be exponentially related to the spacing d.

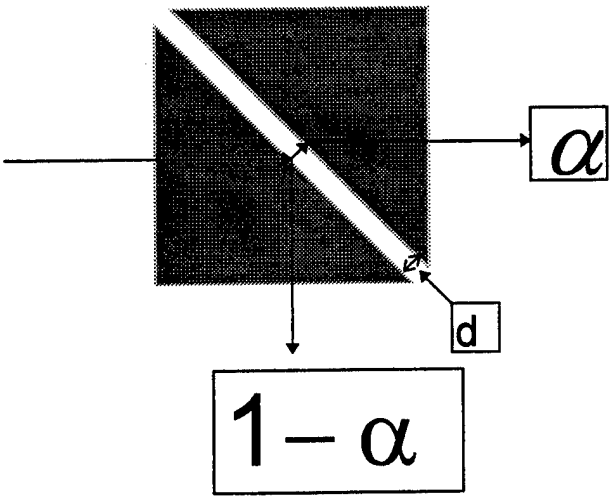

Figure 4-1. Frustrated internal reflection attenuator.

The next step in building a functional variable X-coupler would be to construct a device which will hold the two prisms and apply pressure perpendicular to the hypotenuses of the prisms as shown in Fig. 4-2. The pressure must be evenly distributed on the sides of the prisms to prevent any transverse movement and to prevent cracking the prisms. With a fixed position on one corner of one prism, an adjustable positioner on the corner of the other prism would then push the two hypotenuses together, changing the separation distance. Each positioner would be attached to plates which would distribute the pressure exerted by the positioner over the entire outer face of the prism. Optical windows would have to be inserted into the pressure plates to allow the four light paths needed. The optical windows would simply be large apertures in the plates which would not effect the laser beams.

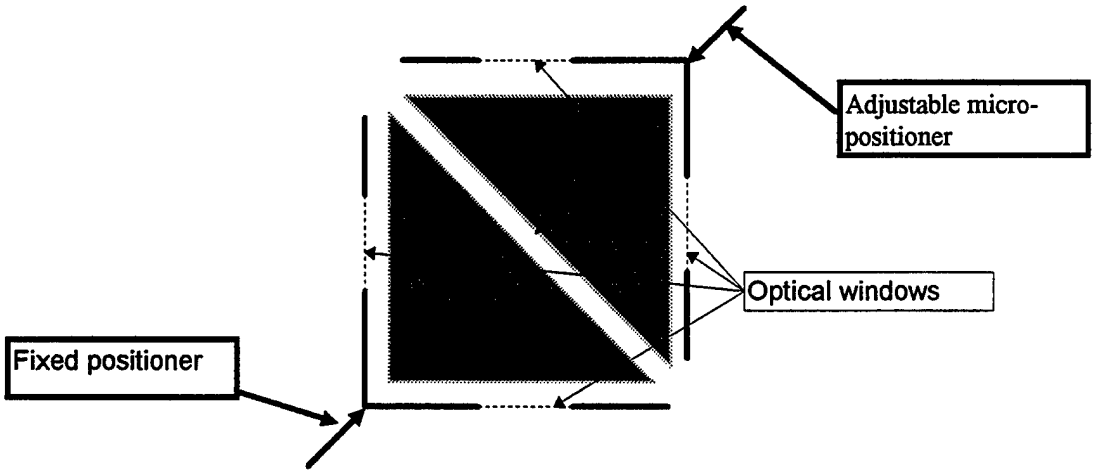

Figure 4-2. X-coupler configuration.

b. Testing the X-Coupler

Two 90^0 bending prisms with anti-reflecting coating with an index of refraction suitable for use with 1.064 μm wavelength have been obtained for use in the variable X-coupler. An experiment using a high power Nd:YAG laser can be completed to verify the ability of the X-coupler to provide a variable ratio split of a single input source. With the Nd:YAG laser output lined up to enter the X-coupler at the E_1 port as shown in Fig. 2-4, power meters will monitor the output of the X-coupler at the E_3 and E_4 ports. As the spacing between the prisms is varied using the micrometer, the data from the power meters will be recorded. With the recorded data, micrometer settings can be calibrated to the expected output ratio.

c. Self-Modulation Theory Experiment

With the X-coupler satisfactorily tested and calibrated, the self-modulation theory can be tested using a variable output power Nd:YAG laser in

the continuous wave mode. With the proper laser, the transmitted and reflected beams from the X-coupler would then be sent into the opposite ends of a single optical fiber. The recombination of the two beams would then be transmitted out of the fourth side of the X-coupler. While slowly varying the input, the output power would be recorded and the results compared to the theoretical output given by a graph similar to Fig. 2-5.

LIST OF REFERENCES

N. J. Doran and D. Wood, *Nonlinear-optical loop mirror*, Optics Letters, Vol. 13, No. 1, pg. 56, January 1988.

R. Guenther, *Modern Optics,* John Wiley & Sons, 1990.

R. C. Harney, *The Rate Equation Theory of Lasers*, Class Notes Naval Postgraduate School Monterey CA, 1996.

M. N. Islam, *Ultrafast Switching With Nonlinear Optics*, Physics Today, pg. 34, May 1994.

F. A. Jenkins and H. E. White, *Fundamentals of Optics, 4th Ed.,* McGraw-Hill Book Company, 1976.

L. D. Landau and E. M. Lifshitz, *Quantum Mechanics: Non-Relativistic Theory,* Addison-Wesley Publishing Company Inc., 1958.

M. C. Ladner, *Optical Modulator LM 0202 P Characteristics: Applications to Amplitude Modulation of Argon-Ion Laser,* Thesis for Master's Degree Naval Postgraduate School Monterey CA, 1996.

A. Larraza and Coleman, *Nonlinear Propagation in Optical Fibers: Applications to Tunable Lasers*, Andrés Larraza, paper prepared for thesis students, 1994.

Lexel Laser Inc., *CW Ion Lasers: Explore the Difference*, Lexel Laser Inc. Ion Laser Specification Sheet, 1996

W. T. Silfvast, *Laser Fundamentals,* Cambridge University Press, 1996.

H. V. Wallace, *Optical Characteristics of Lexel 85 Argon Ion Laser and Gsänger LM0202P Modulator: Application to AM-FM Light Conversion*, Thesis for Master's Degree Naval Postgraduate School Monterey CA, 1996.

INITIAL DISTRIBUTION LIST

1. Defense Technical Information Center.....2
   8725 John J. Kingman Rd., Ste 0944
   Ft. Belvoir, Virginia 22060-6218

2. Dudley Knox Library.....2
   Naval Postgraduate School
   411 Dyer Rd.
   Monterey, California 93943-5101

3. Professor A. A. Atchley, Code PH/Ay.....1
   Department of Physics
   Naval Postgraduate School
   Monterey, California 93943-5002

4. Professor A. Larraza, Code PH/La.....2
   Department of Physics
   Naval Postgraduate School
   Monterey, California 93943-5002

5. Professor Scott Davis, Code PH/Dv.....2
   Department of Physics
   Naval Postgraduate School
   Monterey, California 93943-5002

6. Professor S. Gnanalingam, Code PH/Gm.....1
   Department of Physics
   Naval Postgraduate School
   Monterey, California 93943-5002

7. Professor R.C. Harney, Code Ph/Ha.....1
   Department of Physics
   Naval Postgraduate School
   Monterey, California 93943-5002

8. LCDR Joseph W. Darwood.....2
   13230 Russet Leaf Ln.
   San Diego, California 92129